applied optics

Comparison of the spectral excitation behavior of methane according to InP, GaSb, IC, and QC lasers as excitation source by sensor applications

Tobias Milde,[1,2,*] Morten Hoppe,[1] Herve Tatenguem,[1] Christian Assmann,[1] Wolfgang Schade,[2] and Joachim Sacher[1]

[1]Sacher Lasertechnik GmbH, Rudolf-Breitscheid-Str. 1-5, 35037 Marburg, Germany
[2]Technische Universität Clausthal, Am Stollen 19a, 38640 Goslar, Germany
*Corresponding author: tobias.milde@sacher-laser.com

The MIR wavelength regime promises better gas detection possibilities than the NIR or the visible region because of the higher absorbencies simulated by HITRAN. In the MIR region are many important absorption lines of significant gases, which are relevant in healthcare, production supervision, and safety and environmental monitoring. One of those gases is methane. CH4 shows significant variations in absorbance with a maximum at 3.3 µm, which results in low detection limits in the range of low ppm. Interband-cascade- and quantum-cascade-based lasers emit at higher wavelengths, where the absorbencies of methane are higher. The comparison is done by analyzing the performance of two spectroscopy applications: tunable diode laser absorption spectroscopy and quartz-enhanced photoacoustic spectroscopy.   © 2019 Optical Society of America

1. INTRODUCTION

Molecular gases often show significantly stronger absorption within the mid-infrared (MIR) than in the near-infrared or visible spectral regime. In this MIR region, many important gases have significant absorption lines that are crucial in healthcare, production supervision, and safety and environmental monitoring [1–3]. For this work, we restricted ourselves to methane, which is a major greenhouse gas and a monitor gas for lung cancer [4]. State-of-the-art methane spectroscopy uses laser diodes base on InP material systems that emit around 1650 nm. However, methane shows a poor absorbance below 3 µm, which results int low detection limits in the range of low ppm. Interband cascade (IC)- and quantum cascade (QC)-based laser structures emit in a significantly higher wavelength range, where the simulated absorbencies of methane are about 10^2 times higher than at 1650 nm. Often the exact choice of the wavelength is determined by additional gases in the spectral regime, which may provide disturbances or which are supposed to be determined simultaneously to supply additional information about the investigated system. Of course, those strong absorption lines cannot be used to measure higher concentrations or over long distances. So in summary, every region has its pros and cons depending on the application. Overall, there are four known areas with strong enough absorption lines of methane below 10 µm that we are looking at. They are displayed in Table 1.

For comparison of the spectral excitation behavior at different wavelength regions, the behavior of the detectors at those wavelengths has to be borne in mind. Commercial systems are under high cost pressure. Therefore, costs of sources and detectors compete with sensitivity requirements. The better absorbance beyond 3 µm and poorer sensitivity of the detectors could cancel each other out. Applications to proof the better absorbance in MIR of methane and the performance of the lasers are tunable diode laser absorption spectroscopy (TDLAS) and quartz-enhanced photoacoustic spectroscopy (QEPAS). The measurement data will be presented as well. TDLAS is an accepted technique for industrial process measurement and control, but it depends on the respective detector. Photoacoustic techniques are more specialized on trace gas detection. Photoacoustic techniques detect the gas absorption indirectly by measuring the acoustic waves generated when an excited molecule relaxes. Thus, these techniques are independent detectors for all wavelength regions. Since its development in 2002 by Kosterev et al. [6], QEPAS has been advanced to one of the most sensitive photoacoustic techniques [7–9]. The superior real absorbance of methane is verified by estimating the detection limits.

2. EXPERIMENTAL SETUP

For the sensor application setups, different excitation sources were selected for the different wavelength regions of interest.

Table 1.   Investigated Methane Absorption Lines

Detection Wavelength	Wavenumber	HITRAN Absorbance [5]
1650.96 nm	6057.08 cm^{-1}	$4.5 \cdot 10^{-3} - \ln(I/Io)$
2299.4 nm	4348.93 cm^{-1}	$3.0 \cdot 10^{-4} - \ln(I/Io)$
3301.7 nm	3028.74 cm^{-1}	$1.2 \cdot 10^{-1} - \ln(I/Io)$
8022.72 nm	1246.46 cm^{-1}	$2 \cdot 10^{-2} - \ln(I/Io)$

All diode lasers are specified in the following sections together with their sensor application results. The laser diodes were temperature stabilized, and for these measurements, the submount temperatures, T_{LD}, were controlled with a precision of $T_{LD} = 25°C \pm 0.01°C$. Both measurements were done with variation in gas pressure to get the partial pressures that can be translated to concentrations, as described in the ideal gas law. The integral of each detected signal was calculated for better output accuracy by an optimized field programmable gate array (FPGA) program. This area measurement technique is described with an example of a TDLAS measurement in Fig. 1.

A. TDLAS

The TDLAS measurements were done by projecting the laser light through a 1 m long gas tube, where several gas values such as pressure can be controlled easily. In these experiments, the tube was not heated or cooled so that the gas was held at room temperature. After the gas tube, the optical signal was measured using detectors specified for each wavelength region. It had been recognized that integrals with an area of 50 mV are solvable, so our detection limit was assigned to these. Our TDLAS setup is described in detail in Ref. [11].

B. QEPAS

A schematic of the setup used for automatic measurement of the quartz tuning fork (QTF) resonance frequency (RF) is shown in Fig. 2. It is composed of QTF immersed inside a gas cell, a trans-impedance amplifier (TIA), FPGA, oscilloscope, and analog-to-digital and digital-to-analog converters (ADC/DACs).
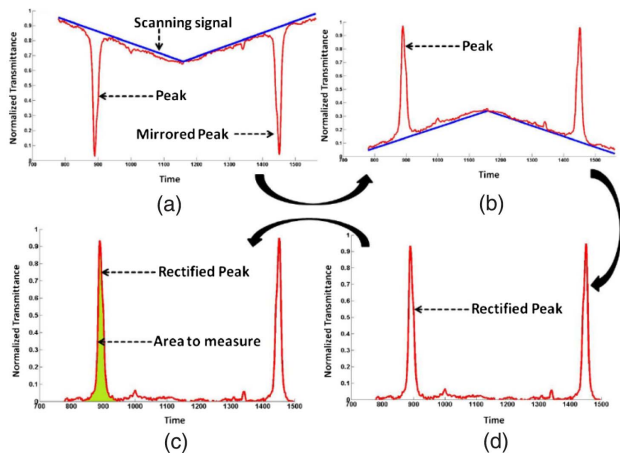

Fig. 1. Steps of the area measurement technique done by the FPGA: (a) acquisition of samples and extraction of the scanning signal. (b) Inversion of transmitted and scanning signals. (c) Peak correction by subtracting the scanning signal. (d) Identification of the section for area measurement [10].
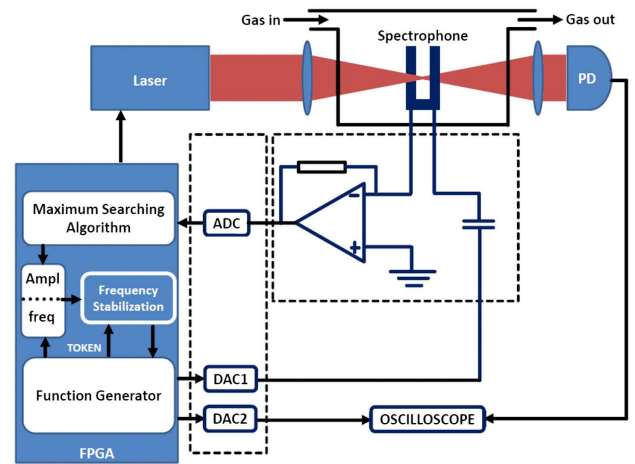

Fig. 2. FPGA setup for automatic detection of the QTF resonance frequency. While measuring the resonance frequency, the laser is turned off.

The QEPAS QTF was enclosed in a compact, vacuum-proven gas cell (10 mm long) where several gas parameters could be controlled [12]. The pressure inside the cell was controlled using a Bourdon pressure gauge. In these experiments, the gas cell was held at room temperature too. The QEPAS measurements were done by focusing the laser light through the gap between the prongs of the bare QTF; in this setup no acoustic micro resonators were used. The QEPAS measurements were done in the $2f$ mode. The gas flowed through the QEPAS cell with a constant flow of 2 cm^3/min, which was controlled by a mass flow controller (MFC). On the exhaust side of the cell, a diaphragm pump was used to stabilize the pressure and concentration inside the QEPAS cell. The pressure/concentration could be adjusted by varying the pump power. Because of the very high signal-to-noise ratio of the QEPAS technique, it had been recognized that integrals with an area of 10 pV were solvable, so our detection limit was assigned to that. Our QEPAS setup and our FPGA analysis process are described in more detail in Ref. [13].

3. RESULTS

For many gases currently measured for medical, industry, safety, and environment reasons, absorption databases such as HITRAN or NIST predict much higher absorbance factors in the MIR than in lower wavelength regions. One of those gases is methane. The HITRAN database says that the absorbance of the absorption band around 3.3 μm is about 10^2 times stronger than the region around 1.65 μm, which is common in current use.

In this work, we concentrate on the four main absorption regions of methane below 10 μm. In both experiments, pure methane was used without a filler gas that could tamper the comparability between the measurements at different wavelengths. That is why the gas concentration had to be varied by the pressure inside the cells. Otherwise, attenuation processes had to be taken into account, which would have needed further complex calibrations. For both experiments, the

integration time was set to 1 s, and 5 spectra were averaged each time. The specific lines that were picked for both applications are shown in Table 1 together with their HITRAN absorbance. The simulation parameters were $T = 300$ K, $P = 1$ bar (760 Torr, 101 kPa), $L = 1$ m, and $\chi = 0.0001$. In this paper, we decided not to display the absorption spectra and the RF curves because the reader should be adequately familiar with them. Examples of those figures can be seen in the above-mentioned references [11,13].

At the end of each subsection, a weighting will take place to estimate the use of these absorption regions and their lasers.

A. 1650 nm

The CH4 R4 lines of the $2\nu 3$ band were measured at a wavelength of 1.651 μm with an InP single-mode laser diode [14]. The characteristics of this digital distributed feedback (DFB) diode laser are shown in Fig. 3, where the PI curve for emission at 1.651 μm is displayed. The attributes of digital laser diodes are described in Refs. [15,16].

The laser threshold is around 20 mA, and the emission power increases to 4 mW with its bias current $I_{\mathrm{bias}} = 140$ mA. In the lower inset, the optical spectrum is shown, while in the upper inset, the tuning behavior of the wavelength over the current is displayed for four different temperatures in steps of 5 K. The temperature tuning range is about $\Delta\lambda = 1$ nm for $\Delta T_{\mathrm{LD}} = 10$ K.

For the CH4 TDLAS measurements at 1.65 μm, the laser bias current was varied around 97 mA with an 11 mA peak-to-peak ramp current modulation. For these measurements, the laser diode temperature was held at $T_{\mathrm{LD}} = 30°C$. Different gas concentrations were adjusted inside the gas tube and measured by the 1.65 μm laser. The light was collected by a home-built InGaAs detector. The analyzed areas of the TDLAS signal at different pressures of methane are displayed in Fig. 4. As one can see, there is quite good linear behavior until 600 mbar CH4. Above 600 mbar, saturation effects emerged and broke
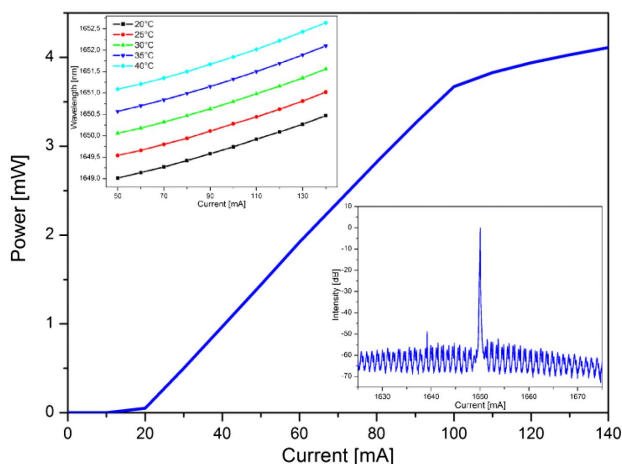

Fig. 4. Methane concentration is displayed as a function of the area of the TDLAS signal. The measurement was done with a DFB laser at 1.65 μm and pressure variation.

the linearity. By extrapolating the signal areas, a detection limit of our measurements can be estimated by using FPGA processing corresponding to former measured area detection limits of the FPGA device with internal amplification. If we had a technique for stably generating very low gas concentrations, we could have detected the CH4 molecules down to a pressure of 0.02 mbar (15 mTorr; 2 Pa) with our setup. This partial pressure can be translated to a concentration of around 20 ppm and a minimum detectivity of 0.1 ppm $\cdot$ mV $\cdot$ Hz$^{-1/2}$. The main limitation of the measurement setup results from the signal-to-noise ratio of the ADC/FPGA detection system. The system as designed is capable of detecting and processing signals up to a minimum of 5 mV at 1 MHz clock rate (CC = clock cycle = 1 μs). That is why the signal areas are specified in voltage per clock cycle (mV.CC).

The calculated integral of the measured CH4 QEPAS spectra are displayed in Fig. 5. As one can see, the variation in pressure is done from 1 bar (770 Torr; 100 kPa) to 50 mbar (37 Torr; 5 kPa). Here, it can be seen that the balance point for CH4 is at 397.7 mbar. This saturation process results from the change of the viscosity of the gas because of pressure reduction. The FPGA extrapolated the signal areas to determine the detection limit of this measurement. Here, CH4 molecules could have been detected down to a pressure of $1.2 \cdot 10^{-4}$ mbar (0.9 mTorr; 0.012 Pa), which means in concentrations around 127 ppb and a minimum detectivity of 0.6 ppb $\cdot$ mV $\cdot$ Hz$^{-1/2}$.

The 1650 nm region of absorption is the present common used area for methane measurements. The absorption is strong enough for detection limits in the low ppm region. In the range of this InP laser, another absorption line at 1648.2 nm (6067 cm^{-1}; $3 \cdot 10^{-3}$ – ln(I/I_o)) is available. This absorption region and the state-of-the-art laser at this wavelength are suitable for, e.g., industrial monitoring where CH4 is produced to the 1.8 ppm methane offset of "normal" air. In this measuring window, there are no strong absorption lines of water vapor, so that measuring damp probes should not be problematic. Strong absorptions for cross sensitivities have C_2H_4 and C_2H_6 in this region.

Fig. 3. P versus I curve for the 1.65 μm centered InP digital DFB laser diode. The wavelength tuning behavior with bias current can be seen in the upper inset for different temperatures. In the lower inset, the measured optical spectrum is shown, with an SMSR value of 48.4 dB.
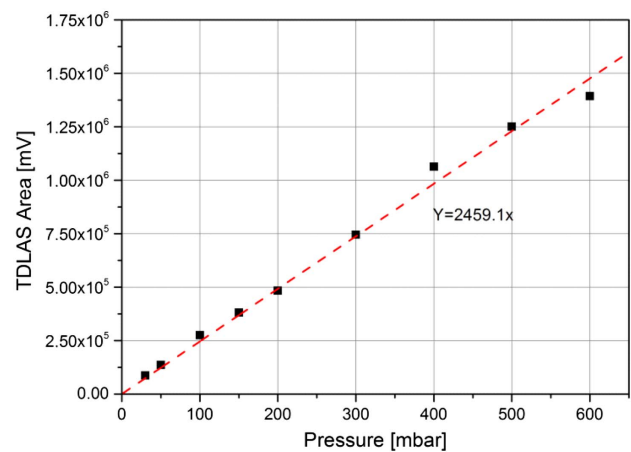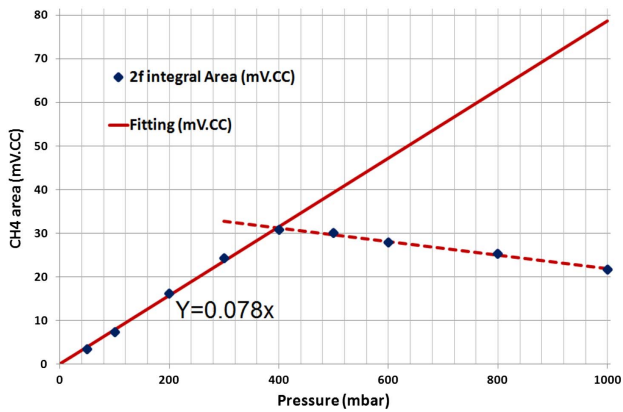
Fig. 5. Area of the QEPAS signal is displayed as a function of the pressure. The zenith of the QEPAS signal has been extrapolated at 397.7 mbar (298.3 Torr; 39.77 kPa).

Fig. 7. Methane concentration is displayed as a function of the area of the TDLAS signal. The measurement was done with a DFB laser at 2.2994 μm and pressure variation.

B. 2300 nm

To measure the methane absorption band around 2.3 μm, we used a newly developed GaSb-based single-mode laser diode. We packaged the digital DFB diode for the measurements and characterized it. The results of this characterization are shown in Fig. 6. As can be seen in Fig. 6, the laser threshold is around 48 mA, and the laser emission power increases with bias current to almost 3.1 mW at $I = 140$ mA. The lower inset shows the optical spectrum. The measured side-mode suppression ratio (SMSR) is 30.3 dB at $I_{bias} = 100$ mA. In the upper inset, the tuning behavior of the wavelength over the current is displayed for five different temperatures in steps of 2.5 K. The current tuning range is around $\Delta\lambda = 1$ nm for ca. $\Delta I_{bias} = 30$ mA. The temperature tuning range is about $\Delta\lambda = 1.17$ nm for $\Delta T_{LD} = 5$ K.

The gas absorption was measured over a wavelength range of 0.67 nm by tuning the laser around 130 mA with a peak-to-peak current modulation of 20 mA in normal conditions.
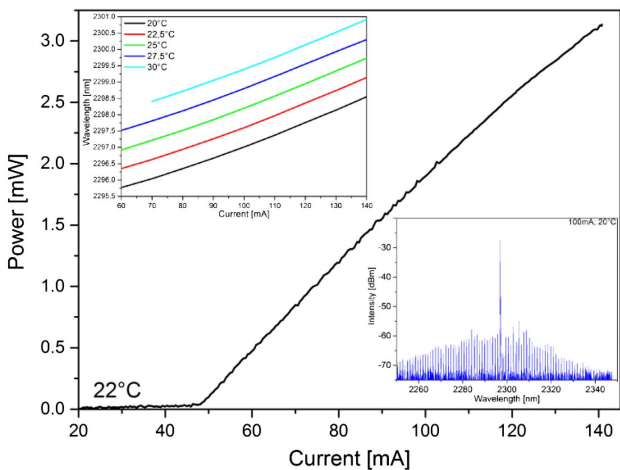
For these measurements, the laser diode temperature was held at $T_{LD} = 25°C$. The light was collected by a home-built extended InGaAs detector. The methane absorption line was located at 2.2994 μm. The integral was also determined, as shown in Fig. 7. Here, CH_4 molecules could have been detected down to a pressure of 0.054 mbar (40 mTorr; 5.4 Pa), which means in concentrations around 54 ppm and a minimum detectivity of 0.27 ppm · mV · Hz$^{-1/2}$.

The QEPAS measurement was done by varying the laser bias current as in the TDLAS measurements. The FPGA analyzed the area of the QEPAS signal here too. It is displayed in Fig. 8 as a function of pressure. It can be seen that the balance point for this wavelength is at 312 mbar (223 Torr; 31.2 kPa). The extrapolation of the signal areas for the detection limit estimation was also done. With this setup, we could have detected molecules down to a partial pressure of $1.98 \cdot 10^{-4}$ mbar (0.15 mTorr; 0.02 Pa), which translates to a concentration of around 198 ppb (1 ppb · mV · Hz$^{-1/2}$).

Fig. 6. P versus I curve for the 2.295 μm centered GaSb Digital DFB laser diode. The wavelength tuning behavior with bias current can be seen in the upper inset for different temperatures. In the lower inset, the measured optical spectrum is shown, with an SMSR value of 30.3 dB.
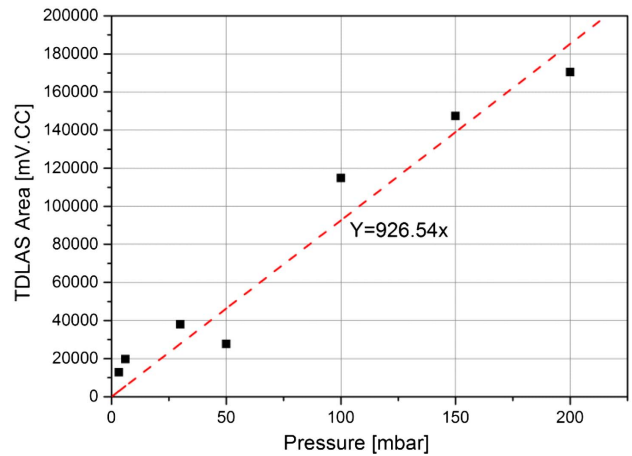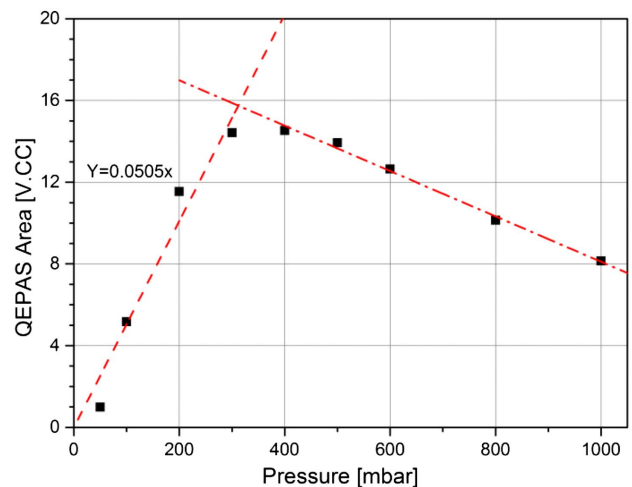

Fig. 8. Area of the QEPAS signal is displayed as a function of the pressure. The zenith of the QEPAS signal has been extrapolated at 312 mbar (223 Torr; 31.2 kPa).

The 2.3 µm region contains absorption lines that are strong enough for detection limits also in the low ppm region. In the range of this GaSb laser, there are several other absorption lines available with lower absorbencies ($4 \cdot 10^{-4}$ – $\ln(I/Io)$ to $3 \cdot 10^{-3}$ – $\ln(I/Io)$). This absorption region and our laser at this wavelength are suitable for a big range of monitoring applications. This can be biogas monitoring where CH_4 is produced to a high percentage level with one of the low absorbance peaks or industrial monitoring with one of the stronger peaks. In this measuring window, there are no strong absorption lines of water vapor, so that measuring damp probes should not be problematic. Strong absorptions in this region have CO and NH_3.

C. 3300 nm

To measure in the very strong absorption region around 3.3 µm we could not use common InP- or GaSb-type lasers because of their well-known power fading beyond emission wavelengths of $\lambda \approx 3$ µm. Beyond 3 µm, only interband cascade lasers (ICLs) or quantum cascade lasers (QCLs) are able to operate with proper performance. In the range of these methane absorption lines, ICLs are superior to laser chips based on the QC design, not to mention the much easier manageability of ICLs [17]. That is because they can operate in voltage ranges like common GaSb-type lasers, and they do not have a great amount of wasted heat that must be gotten rid of.

We packaged a DFB diode with emission centered at 3.298 µm to measure the fundamental absorption band of the CH_4 [18]. The characteristics of this diode are shown in Fig. 9. As can be seen in Fig. 9, the laser threshold is around 75 mA, and the laser emission power increases with bias current to over 5 mW at $I_{bias} = 200$ mA. In the lower inset, the optical spectrum is shown. Due to the fact that an optical spectrum analyzer (OSA) can operate to a wavelength of only around 2.4 µm presently, we had to use Fourier-transform infrared spectros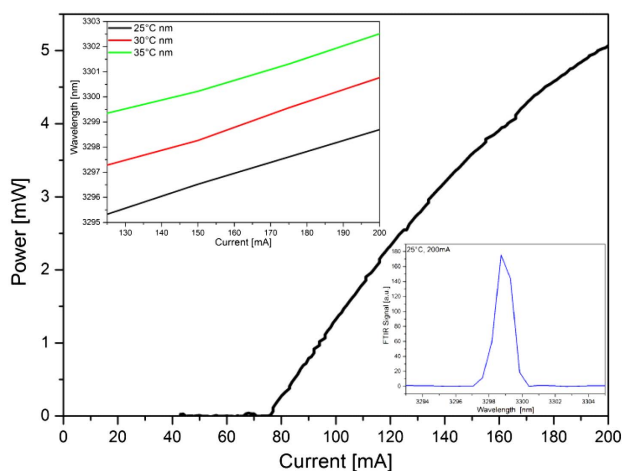copy (FTIR) to determine the wavelength and broadness. Our FTIR has a resolution of just one wavenumber, which explains the bad shape of the spectrum in the lower inset in Fig. 9. Thus, for this instrumental limitation, we refrain from an evaluation of the SMSR. In the upper inset, the tuning behavior of the wavelength over the current is displayed for four different temperatures in steps of 5 K. The current tuning range is around $\Delta\lambda = 1$ nm for $\Delta I_{bias} \sim 22$ mA. The temperature tuning range is about $\Delta\lambda = 2$ nm for $\Delta T_{LD} = 5$ K.

The problem with measuring at such a strong absorption line is the broadening in higher pressures. At standard pressure, the pressure broadening is so strong that the absorption line cannot be seen in the spectra. That is why we had to go far down with the pressure.

For the CH4 TDLAS measurements at 3.298 µm, the laser bias current was varied around 110 mA with a 7 mA peak-to-peak ramp current modulation. For these measurements, the laser diode temperature was held at $T_{LD} = 38°C$. The light was collected by an HgCdTe detector (PVI-6, Vigo). The analyzed areas of the TDLAS signal at different pressures of methane are displayed in Fig. 10. By extrapolating the signal areas, a detection limit for this wavelength can be estimated to $2.3 \cdot 10^{-3}$ mbar (1.7 mTorr; 0.23 Pa) with our setup. This translates to a concentration of around 2.29 ppm and a minimum detectivity of 11 ppb $\cdot$ mV $\cdot$ Hz$^{-1/2}$.

The calculated integrals of the measured CH4 QEPAS spectra at 3.3017 are displayed in Fig. 11. As one can see, the variation in pressure is done as for TDALS in relative low pressure regions from 16 mbar (12 Torr; 1.6 kPa) to 5 mbar (3.7 Torr; 0.5 kPa). Once more, the FPGA extrapolated the signal areas to determine the detection limit of this measurement. Here, CH_4 molecules could have been detected down to a pressure of $1.1 \cdot 10^{-5}$ mbar (7.5 µTorr; 1.1 mPa), which means in concentrations around 10.7 ppb and a minimum detectivity of 0.05 ppb $\cdot$ mV $\cdot$ Hz$^{-1/2}$.

The area around 3.3 µm contains the strongest methane absorption lines that HITRAN knows below 10 µm. The detection limit is in the lower ppb region. In the range of this IC laser, there are also other absorption lines available that are 10^2 times less strong. This absorption region and our laser at this wavelength are suitable for, e.g., breath analysis, where slide fluctuations can indicate cancer in early stages. In this
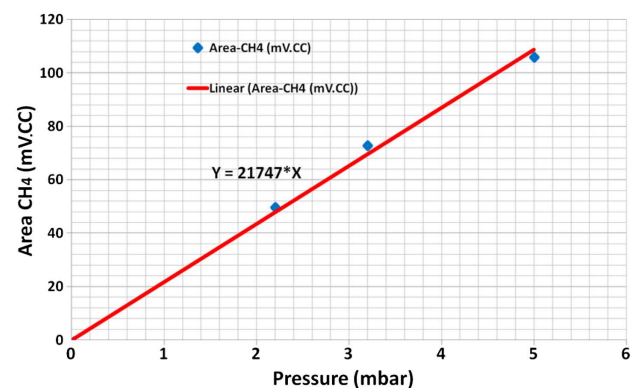
Fig. 9. P versus I curve for the 3.298 µm centered ICL DFB diode. The wavelength tuning behavior with bias current can be seen in the upper inset for different temperatures. In the lower inset, the measured optical spectrum is shown by a low resolution FTIR spectrometer. Thus, for this instrumental limitation, we refrain from an evaluation of the side mode suppression ratio (SMSR).

Fig. 10. Methane concentration is displayed as a function of the area of the TDLAS signal. The measurement was done with a DFB laser at 3.3017 µm and pressure variation.
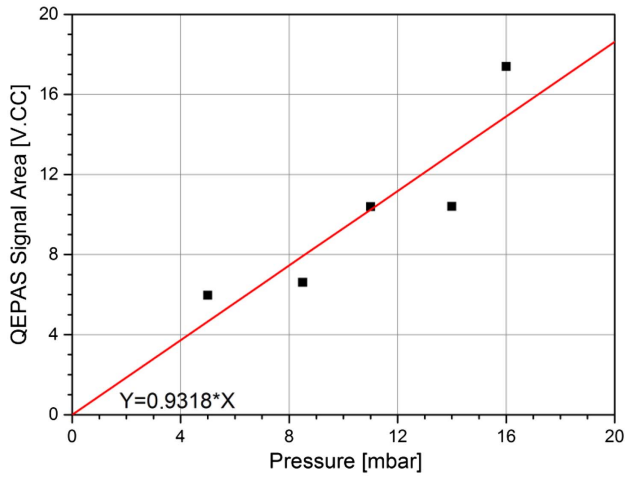
Fig. 11. Area of the QEPAS signal is displayed as a function of the pressure at 3.3017 μm.

Fig. 13. Measured absorption states of methane in the wavelength range of 7.895 μm ≤ λ ≤ 7.935 μm (black curve); calculated HITRAN spectrum by spectraplot.com [5] (red curve) under the same conditions.

measuring window, there are some stronger absorption lines of water vapor, but they do not overlap with the CH_4 lines. Strong absorptions for cross sensitivities have O_3, CH_3Cl, NO_2, C_2H_4, and C_2H_6 in this region.

D. 8021 nm

For higher wavelength regions, we had to use a QCL to measure the absorption of methane. The measurement was also done with another type of laser source than the devices used before. Here, we utilized an external cavity diode laser (ECDL) arrangement that was emitted in a narrow spectrum when operated in the Littman configuration [15,19]. In a Littman configuration, the wavelength can be tuned by adjusting the mirror position relative to the grating by a motor. For measuring methane, we used a QCL-based ECDL where the Fabry–Perot gain block operated at a center wavelength of $\lambda \sim 8.1$ μm. The emission characteristics of this ECDL are shown in Fig. 12.

The laser threshold is $I_{bias} = 1.309$ A, and the laser power can be increased with bias current to a maximum of ca. 90 mW, both near the central wavelength of 8.1 μm. In the upper inset in Fig. 12, the power output over the motor tuning behavior is displayed. By adjusting the mirror in this Littman configuration, the motor can tune the wavelength from nearly 7.8–8.45 μm. In the lower inset, the line width and the side-mode suppression are shown.

By tuning the wavelength of the ECDL with the motor, the gas was scanned over a wavelength range of 40 nm. The measured CH_4 spectrum is displayed in Fig. 13 (black curve). Here, the used detector was a thermal power meter, which also displays the power behavior of the ECDL when wavelength tuned. A trend of increasing power can be noticed due to this effect. The periodic modulation of the power curve is caused by modes hops. For comparison, in Fig. 13 the simulated HITRAN spectrum [5] (red curve) is displayed. As can be seen, the measured and simulated spectra match quite well.

Unfortunately, we could not measure the variation in pressure as shown above. Before finishing enough pressure runs, a component of our pressure-controlling module broke and the repair took too much time to get these measurements into this publication.
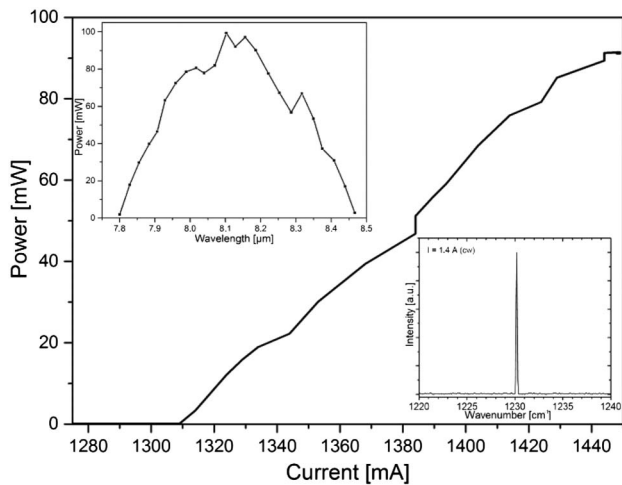

Fig. 12. P versus I curve for the 8.1 μm centered EC QCL. The wavelength motor tuning behavior can be seen in the upper inset. In the lower inset, the measured optical spectrum is shown.
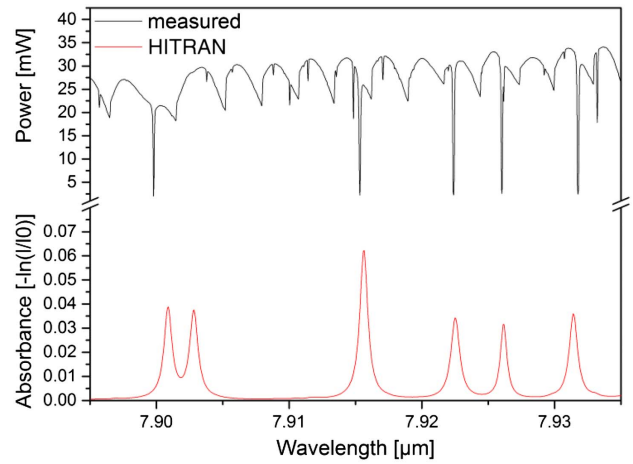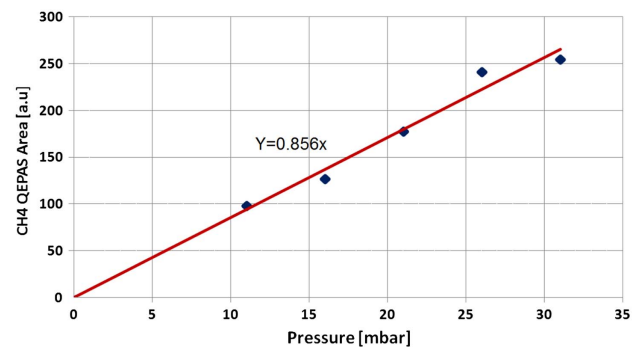

Fig. 14. Area of the QEPAS signal is displayed as a function of the pressure at 8.021 μm.

Table 2.   Investigated Methane Absorption Lines

Detection Wavelength	HITRAN Absorbance	Laser Power	TDLAS Detection Limit	QEPAS Detection Limit
1650.09 nm	$4.5 \cdot 10^{-3} - \ln(I/Io)$	3.5 mW	20 ppm	127 ppb
2299.4 nm	$3.0 \cdot 10^{-3} - \ln(I/Io)$	2 mW	54 ppm	198 ppb
3301.7 nm	$1.2 \cdot 10^{-1} - \ln(I/Io)$	2 mW	2.29 ppm	10.7 ppb
8022.72 nm	$2.0 \cdot 10^{-2} - \ln(I/Io)$	10 mW	To be determent	11.6 ppb

Table 3.   Measurement Factors

	Product Factor	TDLAS Factor	QEPAS Factor
InP/GaSb	2.6	2.7	1.6
ICL/InP	15.2	8.7	11.9
ICL/GaSb	40	23.6	18.5
ICL/QCL	1.2		1.09
QCL/InP	12.6		10.9
QCL/GaSb	33.3		16.9

For QEPAS measurement, it has to be mentioned that by using an ECDL type of laser, the laser was current modulated, and the scan over the QEPAS signal was done by a piezo element that varied the mirror position. The FPGA analyzed the area of the QEPAS signals like before. The result is displayed in Fig. 14 as a function of pressure. The extrapolation of the signal areas for the detection limit estimation shows that we could have detected molecules down to a pressure of $1.16 \cdot 10^{-5}$ mbar (8.7 µTorr; 1.16 mPa), which translates to a concentration of around 11.7 ppb (0.058 ppb $\cdot$ mV $\cdot$ Hz$^{-1/2}$).

The 8.1 µm region of absorption is strong enough for detection limits in the high ppb region. The detection limit is in the low ppb region. In the range of this IC laser, there are also other absorption lines available that are 10^2 times less strong. This absorption region and our laser at this wavelength are suitable for, e.g., environmental monitoring where CH_4 fluctuations can be observed around the 1.8 ppm offset of "normal" air. In this measuring window, there are a few stronger absorption lines of water vapor, but they do not overlap with the CH_4 lines. Strong absorptions for cross sensitivities have CO_2, COF_2, C_2H_2, HCO_2H, HNO_3, H_2O_2, NH_3, H_2S, N_2O, O_3, PH_3, and SO_2 in the region of this laser.

4. CONCLUSION

This work shows the methane absorption behavior over the four common used absorption lines. For many scientists, this investigation is a decision support with which wavelength their measurement system is at best. Not always the strongest line is the best choice. Cross sensitivities and simultaneous detection of more than one gas has to be kept in mind as well as costs for sources and detectors.

The results of both applications are collated for each wavelength in Table 2. The absorbencies from the HITRAN database are also shown in Table 2 as the laser power at the investigated methane absorption line.

We know from the Lambert–Beer law that absorbance is linear to the absorption coefficient and in a first approximation, disregarding higher-order effects, to the laser power. So by making the product of the absorbance factor and laser power factor,

the factor of the detection limit ratio should appear if the other values of Lambert–Beer (e.g., path length) are held equal.

When we first look at the TDLAS measurements, the determined ratio (factor 2.7) of the detection limits of the measurements below 3 µm correlate with the ratios from the product of the absorbencies (factor 1.5) and laser power (factor 1.75). The same is done with the 2.3 µm and 3.3 µm measurements. The detection limit ratio (factor 23) is half of the ratio product from the absorbencies (factor 40) and laser power (factor 1). All factors are collected in Table 3.

As one can see in Table 3 for the ratios between 1.65 µm and 2.3 µm, the detection limit ratio is 2.7 and the product of the factors is 2.6. Both factors match quite well. For the other two comparisons, the accordance is not as good as with 1.65 µm and 2.3 µm but in the same dimension. The discrepancies can be explained by the different efficiencies of used detector materials, the dependence of the attenuation coefficient upon the wavelength, and other uncertainties of the measurements.

The detection limits that were determined with the QEPAS technique should be easily comparable to each other. That is because here the different detector material uncertainties do not impact. Here also the QCL can be used to verify the data. Caused by its building technique and the high amount of wasted heat, the distance to the sample cell was higher than with the DFB laser, so laser power was extenuated to those 10 mW mentioned in Table 2. As can be seen in Table 3, the comparability of the QEPAS factors is as good as with the TDLAS factors. The calculated factors match both times quite well, except most measurements with the GaSb laser (beside InP/GaSb), which are half as high as the product factors.

REFERENCES

1. C. Wang and P. Sahay, "Breath analysis using laser spectroscopic techniques: breath biomarkers, spectral fingerprints, and detection limits," Sensors **9**, 8230–8262 (2009).

2. R. Liang, J. Chen, G. Kipshidze, D. L. Shterengas, and G. Belenky, "High-power 2.2 µm diode lasers with heavily strained active region," IEEE Photon. Technol. Lett. **23**, 603–605 (2011).

3. Y.-Z. Song, Y. Zhang, J.-K. Song, K.-W. Li, Z.-Y. Zhang, Y. Xu, G.-F. Song, and L.-H. Chen, "Single mode 2 µm GaSb based laterally coupled distributed feedback quantum-well laser diodes with metal grating," Chin. Phys. Lett. **32**, 074206 (2015).

4. M. Phillips, K. Gleeson, M. B. Hughes, J. Greenberg, R. N. Cataneo, L. Baker, and P. McVay, "Volatile organic compounds in breath as markers of lung cancer: a cross-sectional study," Lancet **353**, 1930–1933 (1999).

5. "HITRAN spectra simulation website," http://spectraplot.com.

6. A. A. Kosterev, Y. A. Bakhirkin, R. F. Curl, and F. K. Tittel, "Quartzenhanced photoacoustic spectroscopy," Opt. Lett. **27**, 1902–1904 (2002).

7. M. Mordmueller, W. Schade, and U. Willer, "QEPAS with electrical coexcitation for photoacoustic measurements in fluctuating background gases," Appl. Phys. B **123**, 224 (2017).

8. Y. Ma, "Review of recent advances in QEPAS-based trace gas sensing," Appl. Sci. **8**, 1822 (2018).

9. P. Patimisco, A. Sampaolo, L. Dong, F. K. Tittel, and V. Spagnolo, "Recent advances in quartz enhanced photoacoustic sensing," Appl. Phys. Rev. **5**, 011106 (2018).

10. T. Milde, M. Hoppe, H. Tatenguem, W. Schade, and J. Sacher, "Comparison of the spectral excitation behavior of methane according to InP, IC and QC lasers as excitation source by sensor applications," in *Photonics West SPIE Opto Conference* (2019).

11. T. Milde, C. Assmann, A. Jimenez, M. Honsberg, J. O'Gorman, W. Schade, and J. Sacher, "Single mode GaSb diode lasers for sensor applications in a long wavelength regime," Appl. Opt. **56**, H45–H50 (2017).

12. M. Mordmüller, M. Köhring, W. Schade, and U. Willer, "An electrically and optically cooperated QEPAS device for highly integrated gas sensors," Appl. Phys. B **119**, 111–118 (2015).

13. T. Milde, M. Hoppe, H. Tatenguem, M. Mordmüller, J. O'Gorman, U. Willer, W. Schade, and J. Sacher, "QEPAS sensor for breath analysis: a behavior of pressure," Appl. Opt. **57**, C120–C127 (2018).

14. H. Huang and K. K. Lehmann, "Long-term stability in continuous wave cavity ringdown spectroscopy experiments," Appl. Opt. **49**, 1378–1387 (2010).

15. A. Jimenez, T. Milde, N. Staacke, C. Assmann, J. O'Gorman, and J. Sacher, "Narrow-line diode laser packaging and integration in the NIR and MIR spectral range," Proc. SPIE **10085**, 1008505 (2017).

16. T. Milde, A. Jimenez, J. R. Sacher, and J. O'Gorman, "Long wavelength single mode GaSb diode lasers for sensor applications," in *Conference on Lasers and Electro-Optics*, OSA Technical Digest (Optical Society of America, 2017), paper JTu5A.111.

17. I. Vurgaftman, R. Weih, M. Kamp, J. R. Meyer, C. L. Canedy, C. S. Kim, M. Kim, W. W. Bewley, C. D. Merritt, J. Abell, and S. Höfling, "Interband cascade lasers," J. Phys. D **48**, 123001 (2015).

18. A. A. Popov, M. V. Stepanov, V. V. Sherstnev, and Y. P. Yakovlev, "3.3-mm LEDs for measuring methane," Tech. Phys. Lett. **23**, 828–830 (1997).

19. S. Stry, S. Thelen, J. Sacher, D. Halmer, P. Hering, and M. Mürtz, "Widely tunable diffraction limited 1000 mW external cavity diode laser in Littman/Metcalf configuration for cavity ring-down spectroscopy," Appl. Phys. B **85**, 365–374 (2006).